Chapter 3

Active nematic gel with quenched disorder

3.1 Introduction

In the previous chapter (**Chapter 2**), we have studied the effect of quenched disorder on the dry active nematics, i.e., dry-RFAN [Kumar & Mishra (2020)], where we have ignored the effect of the background fluid. But, the effect of the fluid in which apolar active particles are suspended can not always be neglected; the suspension of microtubules with molecular motors in oil and colonies of Myxococcus xanthus are some of the examples of wet active nematics or active nematic gel [Copenhagen et al. (2021); Doostmohammadi et al. (2016a)]. Therefore, the impact of quenched disorder in wet active nematic can also be interesting, and we will address the problem in this work.

We use the same approach to study the effect of quenched disorder in active nematics suspended in an incompressible fluid, as in chapter 2. We write coarse-grained hydrodynamic equations of motion for the sow variables, density, and the orientation field. To see the effect of fluid, we

add one more equation for the flow of the fluid, analogous to the Naiver-Stokes equation as given in [Giomi et al. (2011, 2013)]. The quenched disorder is introduced in the same way as in [Kumar & Mishra (2020)]. Results from the the numerical simulation suggests that the finite disorder slows the ordering kinetics and the effect of disorder is almost the same for both contractile and extensile cases (discussed later). The effect of disorder on the two-point correlation function is substantial, and the system does not show static scaling; in contrast, it is minimal on the density correlation function. Further, the system shows dynamics scaling for the non-zero disorder. We also find that the density growth is faster than the nematic order parameter, which was not found in the dry RFAN [Kumar & Mishra (2020)].

We organize the work as follows: we introduce the model of our system in Sec. 3.2, then we discuss the results Sec. 3.3, and summarize the results in Sec. 3.4.

3.2 Model and Numerical details

We write the hydrodynamic equations of motion for active nematic suspended in an incompressible fluid referred as "active nematic gel". We study the effect of quenched disorder on the system kinetics. These equations are formulated in terms of local density field ρ, flow field $\mathbf{v}$, and the nematic order parameter $\mathscr{Q}_{ij} = S(n_i n_j - \frac{1}{2}\delta_{ij})$, where $\mathbf{n}$ is the director field and $i = 1, 2$ in two dimensions. $\mathscr{Q}_{ij}$ is traceless and symmetric and hence have only two independent components in two dimensions. The disorder in the system is added to the $\mathscr{Q}$ equation only.

For simplicity we write the hydrodynamic equation of motion for incompressible fluid, i.e. $\nabla \cdot \mathbf{v} = 0$. The density equation is given as,

$$[\partial_t + v_i\partial_i]\rho = \partial_i[(D_0\delta_{ij} + D_1\mathscr{Q}_{ij})\partial_j\rho + \alpha_1\rho^2\partial_j\mathscr{Q}_{ij}], \tag{3.1}$$

the equation for the flow field is,

$$[\partial_t + v_i\partial_i]v_i = \eta\partial_i^2 v_i - \partial_i p + \partial_j\tau_{ij}, \tag{3.2}$$

and finally, the equation for the orientation or the nematic order parameter field is give as,

$$[\partial_t + v_i\partial_i]\mathscr{Q}_{ij} = \lambda S u_{ij} + \mathscr{Q}_{ik}\omega_{kj} - \omega_{ik}\mathscr{Q}_{kj} + \gamma^{-1}\mathscr{H}_{ij} + H'_{ij} \tag{3.3}$$

where, $(D_0\delta_{ij} + D_1\mathscr{Q}_{ij})$ is the anisotropic diffusion coefficient term with constant D_0 and D_1. η, p and λ are the viscosity, pressure and the nematic alignment parameter respectively. Here, $u_{ij} = \frac{1}{2}(\partial_i v_j + \partial_j v_i)$ and $\omega_{ij} = \frac{1}{2}(\partial_i v_j - \partial_j v_i)$ are the symmetrized rate of strain tensor and vorticity, respectively. The molecular field $\mathscr{H}_{ij}$ embodies the relaxational dynamics of the nematic phase (with γ a rotational viscosity) and can be obtained from the variation of the Landau-de Gennes free energy of a two-dimensional nematic, $\mathscr{H}_{ij} = -\frac{\delta\mathscr{F}}{\delta\mathscr{Q}_{ij}}$, with

$$\frac{\mathscr{F}}{K} = \int dA[\tfrac{1}{4}(\rho - \rho_0)tr\mathscr{Q}^2 + \tfrac{1}{4}\rho(tr\mathscr{Q}^2)^2 + \tfrac{1}{2}|\nabla\mathscr{Q}|^2] \tag{3.4}$$

where, K is an elastic constant with dimensions of energy, ρ_0 is the critical density for isotropic-nematic transition, so that at an ordered steady state, $S = \sqrt{1-\frac{\rho_0}{\rho}}$. The quenched disorder is introduced as *random field* in the free energy density $\mathscr{F} = -\mathscr{Q} : (\mathbf{hh} - \frac{\mathbf{I}}{2})$. Which further leads to $H'_{ij} = (h_i h_j - h_0^2 \frac{1}{2}\delta_{ij})$, in equation 3.2, in two-dimensions $i, j = 1, 2$ are the spatial indices for the two components of vectors. Where, $h_i = h_0(cos\phi, sin\phi)$, here h_0 is the disorder strength and $\phi(\mathbf{r})$ is a uniform random angle between $(0, 2\pi)$, with mean zero, quenched in time (no time dependence) and space correlation $\langle \phi(\mathbf{r})\phi(\mathbf{r}')\rangle = \delta(\mathbf{r}-\mathbf{r}')$. Finally the stress tensor $\sigma_{ij} = \sigma^r_{ij} + \sigma^a_{ij}$ is the sum of the elastic stress due to nematic elasticity, $\sigma^r_{ij} = -\lambda S\mathscr{H}_{ij} + \mathscr{Q}_{ik}\mathscr{H}_{kj} - \mathscr{H}_{ik}\mathscr{Q}_{kj}$, $\sigma^a_{ij} = \alpha_2\rho^2\mathscr{Q}_{ij}$ is the active contribution, further, it describes contractile or extensile stresses exerted by the active particles in the direction of the director field. Activity yield a curvature induced active current $\mathbf{j}_a = \alpha_1\rho^2\nabla\cdot\mathscr{Q}$ in equation 3.1. The ρ^2 dependence of the active stress and current is appropriate for systems where activity arises from pair interactions among the filaments via cross-linking motor proteins. The sign of α_2 depends on whether the active particles generate contractile or extensile stresses, with $\alpha_2 > 0$ for the contractile case and $\alpha_2 < 0$ for extensile systems, while we always keep $\alpha_1 > 0$. The Eqs. (3.1 - 3.3) written in dimensionless units by rescaling all lengths by the length of the particle and time by the collision time and are of the same form as derived from the microscopic rule-based model in [Bertin et al. (2013)], with fluid flow [Giomi et al. (2011, 2013)] and an additional term due to *quenched disorder* as in the dry case [Kumar & Mishra (2020)]. The random field introduced in our current model is similar to the random field in XY-model (RFXY-model) [Imry & Ma (1975)]. Hereafter we refer our model as random field wet active nematic or RFWAN when $h_0 \neq 0$, and clean-wet active nematic (clean-WAN) for $h_0 = 0$.

To perform the numerical integration of Eqs. 3.1 and 3.2 we construct a two-dimensional $K \times K$ square lattice with periodic boundary condition (PBC) and discretise the space and time derivatives using Euler scheme ($\Delta x = 1.0$ and $\Delta t = 0.1$). Initially, we start with random

homogeneous density, with mean ($\rho_0 = 0.75$), random orientation and flow field. Coarsening is studied for $K = 1024$. Coarsening results are obtained for simulation time $t = \mathcal{O}(10^4)$ and the average over 10 independent realisations. One simulation time is counted after update of Eqs. 3.1 - 3.3 for all lattice points. Parameters in Eqs. (3.1-3.3) are $\alpha_1 = 0.2$ $|\alpha_2| = 2a_1$, $D_0 = 1.0,\ D_1 = 0.5,\ \gamma = 1.0,\ \lambda = 0.1,\ \eta = 2.0$.

3.3 Results

3.3.1 Sapshots

We first generate the time evolution of the system. We show the snapshots for the local nematic order parameter (NOP) field $\mathscr{Q}_{ij}(\mathbf{r},t)$, local density field $\rho(\mathbf{r},t)$, and flow field $\mathbf{v}(\mathbf{r},t)$ and plotted in Fig. 3.1 at different simulation time. These snapshots show the time evolution of different fields throughout the system. Also, we can see the topological defects of two equal and opposite charges, i.e., $\pm 1/2$ defects. These defects attract each other due to the equal and opposite charge, where the $+1/2$ defects have an asymmetric comet-like structure and make it motile. In contrast, the $-1/2$ defect has threefold symmetry and can only diffuse in the system. We observe that as time progresses, the defects annihilation leads to the formation of ordered domains. In the ordered steady state, the system does not have any defect pair, and the value of local fields will be homogeneous throughout the system. Fig. 3.2 show the snapshots of local NOP $\mathscr{Q}(\mathbf{r},t)$ at different time for different strengths of disorders, h_0 and $\alpha_2 < 0$. First observation from these snapshots is that for a fixed non-zero disorder ($h_0 = 0.2$), the number of topological defects or the $\pm 1/2$ defects pairs are larger, Fig. 3.2(bottom panel) compare to the zero disorder case ($h_0 = 0.0$) shown in Fig. 3.2(top panel). Further, this scenario remains unchanged as time evolves. Hence, for a non-zero disorder, the annihilation of $\pm 1/2$ defect pairs is slower than zero disorder.

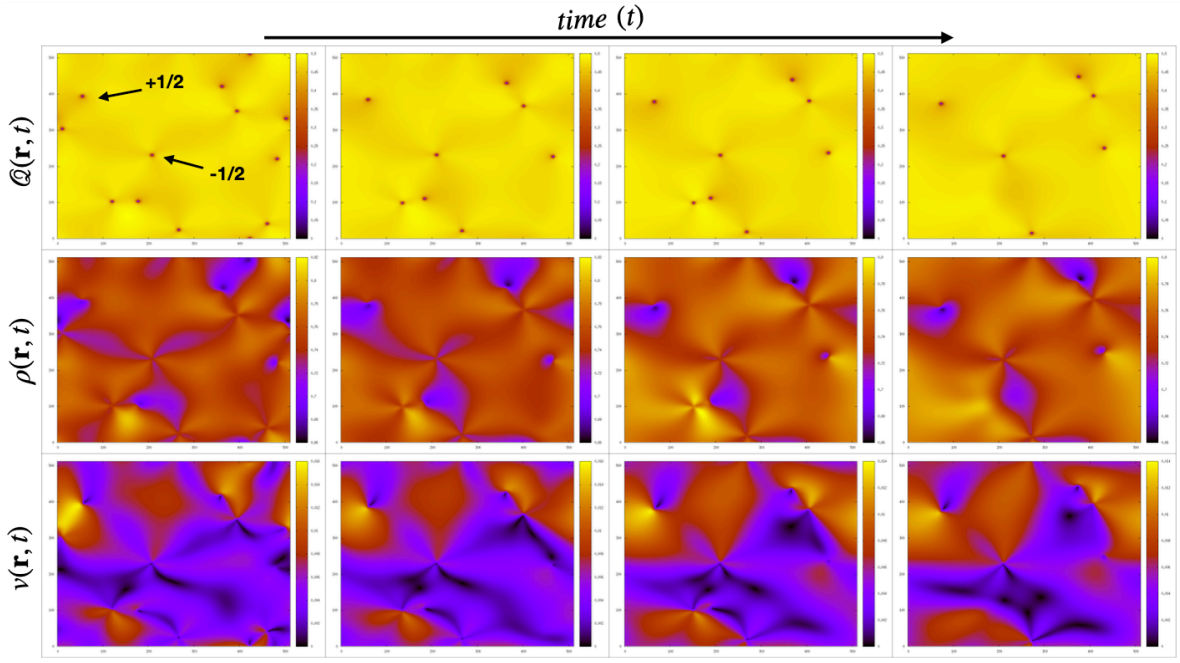

Fig. 3.1 Snapshots at different time for $\alpha_2 < 0$ and $h_0 = 0.0$. Different snapshots are for (NOP) field $\mathscr{Q}(\mathbf{r},t)$ (top panel), local density field $\rho(\mathbf{r},t)$ (middle panel), and flow field $\mathbf{v}(\mathbf{r},t)$ (bottom panel).A pair of $+1/2$-defect and $-1/2$-defect are indicated by the arrows in the first picture (top left). The range of color bars for NOP, density and flow fields are in range $(0.0,0.5)$, $(0.0,0.82)$ and $(0.0,0.016)$, respectively.

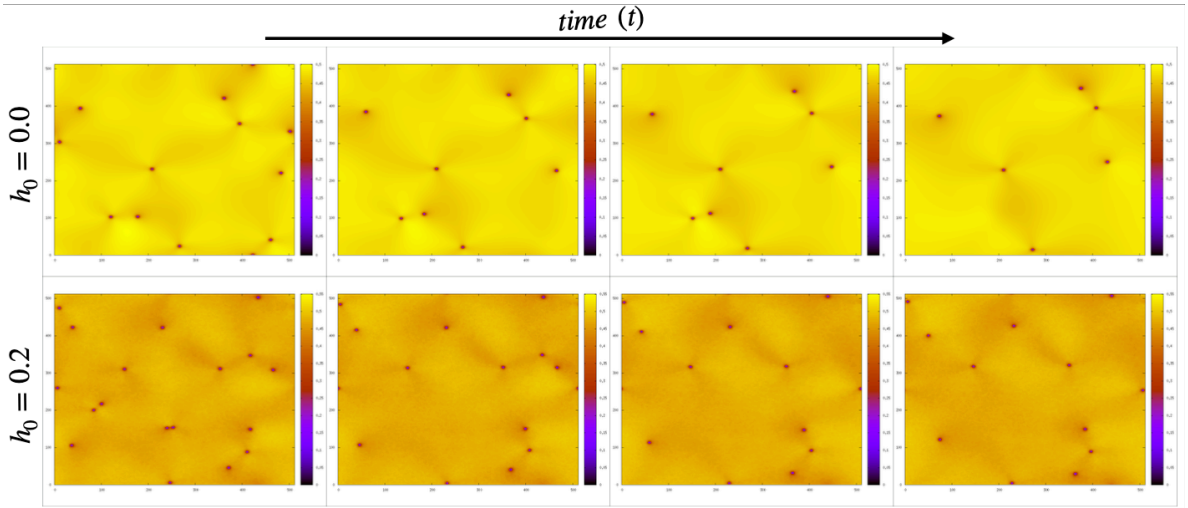

Fig. 3.2 Snapshots of NOP $\mathscr{Q}(\mathbf{r},t)$ at different time for $\alpha_2 < 0$; for different disorder strengths $h_0 = 0.0$ (top panel) and $h_0 = 0.2$ (botom panel). Range of the color bars are same as given for fig. 3.1.

3.3.2 Kinetics

We calculate the two point correlation functions for orientation and density fields, $C_{\mathscr{Q},\rho}$, defined as, $C_{\mathscr{Q}}(\mathbf{r},t) = \langle \mathscr{Q}(\mathbf{0},t) : \mathscr{Q}(\mathbf{r},t) \rangle$ and, local density ρ, $C_{\rho}(\mathbf{r},t) = \langle \delta\rho(\mathbf{0},t)\delta\rho(\mathbf{r},t) \rangle$, where $\delta\rho(\mathbf{r},t) = \rho(\mathbf{r},t) - \rho_0$ is the deviation of the local density from the mean ρ_0. Fig. 3.3 shows the plot for $C_{\mathscr{Q},\rho}(\mathbf{r},t)$ vs. r for different h_0 and at fixed t, and find that the correlation among the particles decreases as we increase the disorder, for both contractile ($\alpha_2 > 0$) and exensile ($\alpha_2 < 0$) cases. In fig. 3.4 and fig. 3.5, we again plot the correlation function for fixed disorder and different simulation time and observe increase in $C_{\mathscr{Q},\rho}(\mathbf{r},t)$ as the time evolve for all disorders.

To understand the effect of quenched disorder on the ordering kinetics, we calculate the correlation length for density ($L_{\rho}(t)$) and order parameter fields ($L_{\mathscr{Q}}(t)$) and plot it for different strength of disorders, h_0. Fig. 3.6, shows the plots of correlation lengths, $L_{\mathscr{Q},\rho}(t)$ vs. time t for different strengths of disorder, h_0. We observe that the correlation length (or the size of ordered domain), decreases as we increase the disorder in the system. The impact of disorder is similar for both contractile ($\alpha_2 > 0$) and extensile ($\alpha_2 < 0$) cases. Further, in fig. 3.7, we plot $L_{\mathscr{Q},\rho}(t)$ vs. time with logarithmic correction $t/ln(t)$ on $log - log$ scale, and find that the correlation length grows as $L_{\mathscr{Q},\rho}(t) \sim [t\ln(t)]^{1/z}$, where z is called as the growth exponent [Bray (1994)]. We observe that the value of z^{-1} decreases gradually as we increase the disorder strength h_0. We study the scaling properties of the two point correlation functions $C_{\mathscr{Q},\rho}(r/L_{\mathscr{Q},\rho}(t))$ where the distance r is scaled as $r/L_{\mathscr{Q},\rho}(t))$, in fig. 3.8, 3.9 and 3.10. From these plots we observe that the system shows good dynamics scaling as the data collapse to a single curve for different time and fixed h_0, see fig. 3.9 and 3.10. Further, the system failed to show static scaling for different disorder and fixed t, see fig. 3.8.

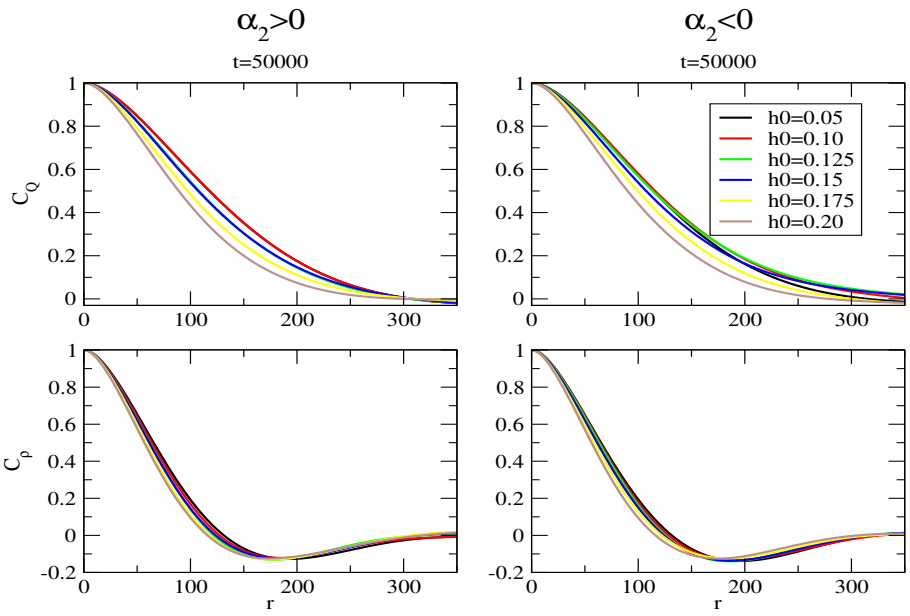

Fig. 3.3 Two point correlation function, $C_{\mathscr{Q}}$ vs. r (top-left and top-right) and C_ρ vs. r (bottom-left and bottom-right) for different h_0. All the data shown are at fixed simulation time $t = 50000$. Plot in left panel plots are for contractile case with $\alpha_2 = 0.4$, whereas right panel shows the plots for extensile case with $\alpha_2 = -0.4$.

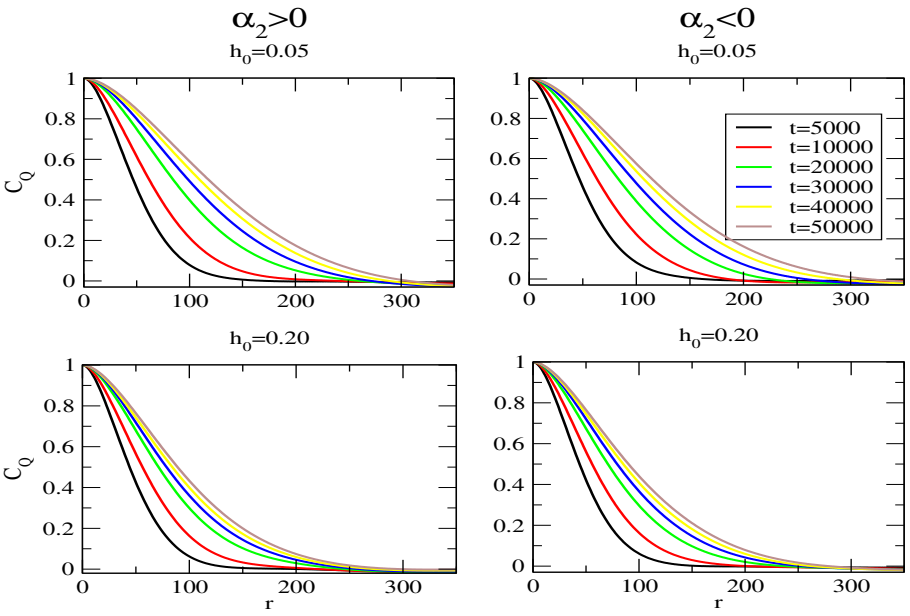

Fig. 3.4 Two point correlation function, $C_{\mathscr{Q}}$ vs. r for $h_0 = 0.05$ (top-left and top-right), and $h_0 = 0.2$ (bottom-left and bottom-right) for different t. Plot in left panel plots are for contractile case with $\alpha_2 = 0.4$, whereas right panel shows the plots for extensile case with $\alpha_2 = -0.4$.

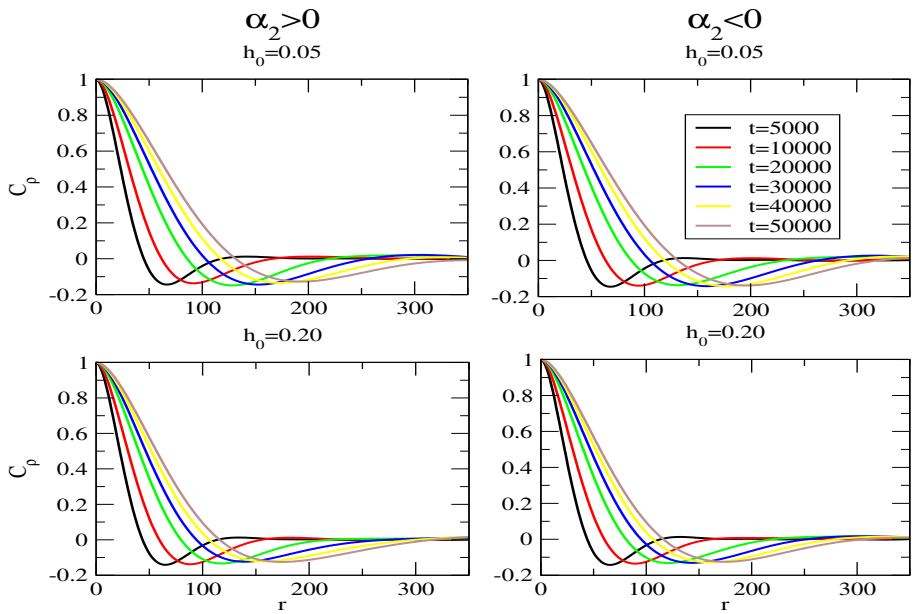

Fig. 3.5 Two point correlation function, C_ρ vs. r for $h_0 = 0.05$ (top-left and top-right), and $h_0 = 0.2$ (bottom-left and bottom-right) for different t. Plot in left panel plots are for contractile case with $\alpha_2 = 0.4$, whereas right panel shows the plots for extensile case with $\alpha_2 = -0.4$.

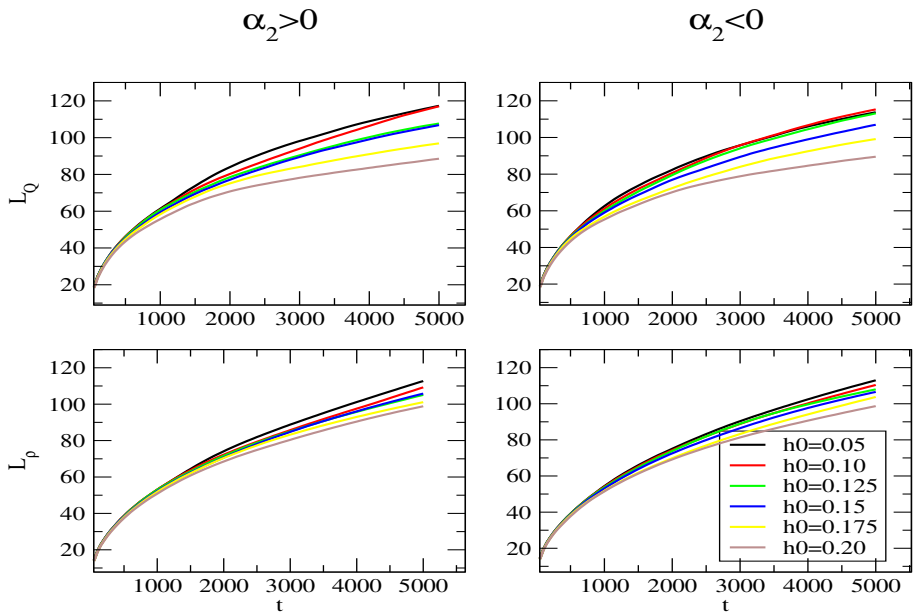

Fig. 3.6 Correlation length, $L_{\mathscr{Q}}$ vs. t (top-left and top-right) and L_ρ vs. t (bottom-left and bottom-right) for different h_0. Plot in left panel plots are for contractile case with $\alpha_2 = 0.4$, whereas right panel shows the plots for extensile case with $\alpha_2 = -0.4$.

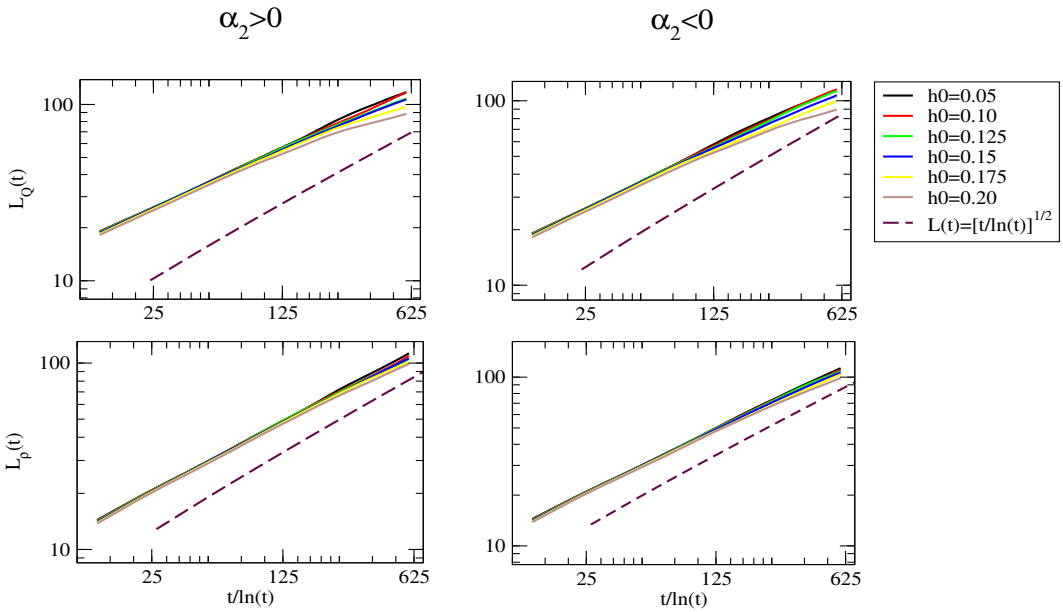

Fig. 3.7 Correlation length, $L_{\mathscr{Q}}$ vs. $t/ln(t)$ (top-left and top-right) and L_ρ vs. t (bottom-left and bottom-right) for different h_0 (log-log scale). Plot in left panel plots are for contractile case with $\alpha_2 = 0.4$, whereas right panel shows the plots for extensile case with $\alpha_2 = -0.4$. Dashed line corresponds to correlation length in equilibrium $xy-model$

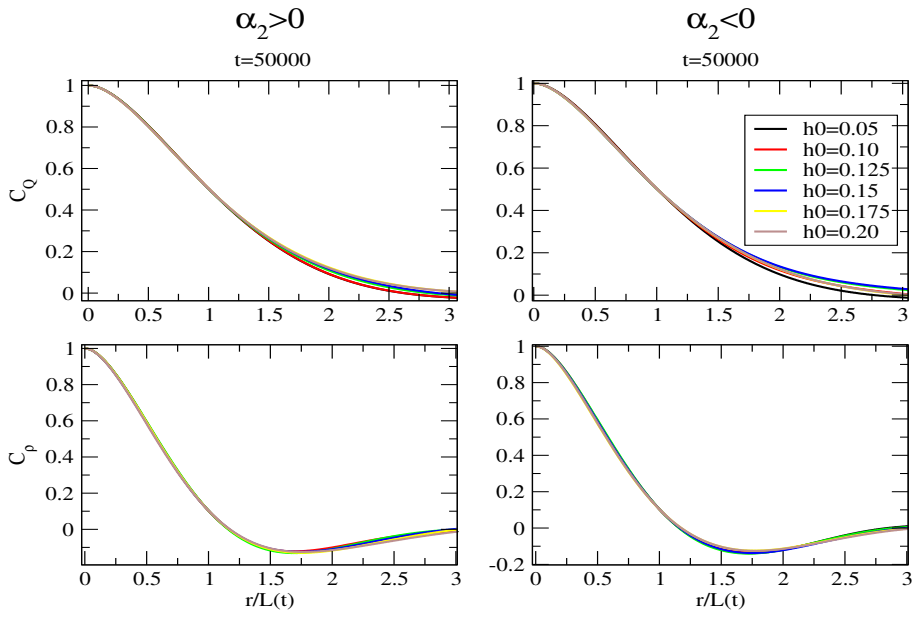

Fig. 3.8 Scaled two point correlation function, $C_{\mathscr{Q}}$ vs. r (top-left and top-right) and C_ρ vs. r (bottom-left and bottom-right) for different h_0. x-axis is scaled as $r \to r/L_{\mathscr{Q},\rho}(t)$. All the data shown are at fixed simulation time $t = 50000$. Plot in left panel plots are for contractile case with $\alpha_2 = 0.4$, whereas right panel shows the plots for extensile case with $\alpha_2 = -0.4$.

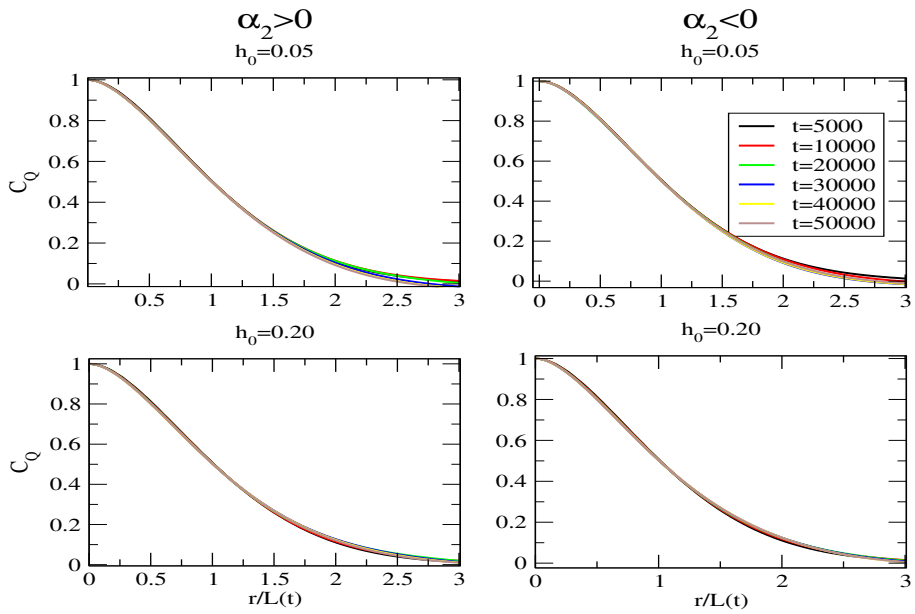

Fig. 3.9 Scaled two point correlation function, $C_{\mathscr{Q}}$ vs. r for $h_0 = 0.05$ (top-left and top-right), and $h_0 = 0.2$ (bottom-left and bottom-right) for different t. x-axis is scaled as $r \to r/L_{\mathscr{Q},\rho}(t)$. Plot in left panel plots are for contractile case with $\alpha_2 = 0.4$, whereas right panel shows the plots for extensile case with $\alpha_2 = -0.4$.

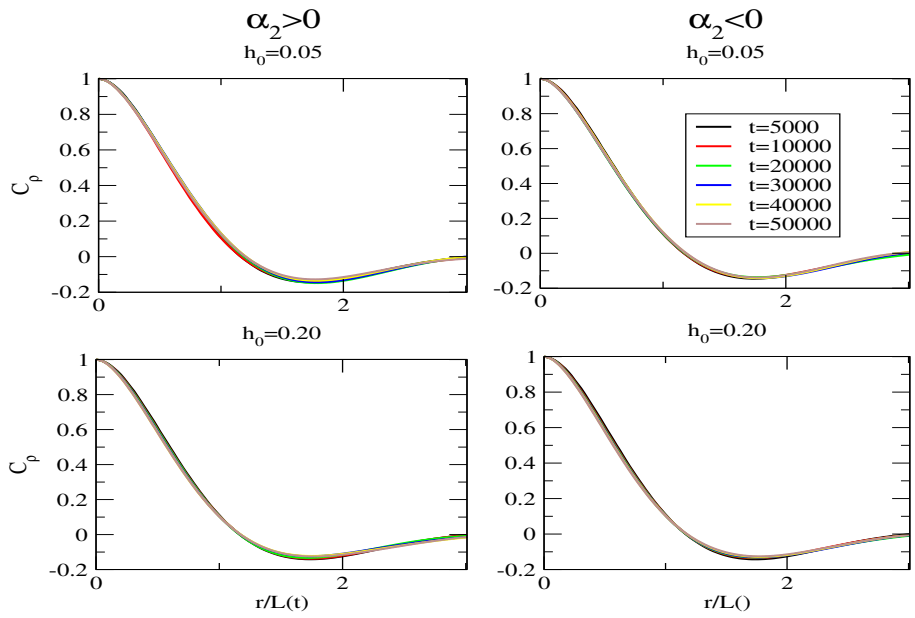

Fig. 3.10 Scaled two point correlation function, C_ρ vs. r for $h_0 = 0.05$ (top-left and top-right), and $h_0 = 0.2$ (bottom-left and bottom-right) for different t. x-axis is scaled as $r \to r/L_{\mathscr{Q},\rho}(t)$. Plot in left panel plots are for contractile case with $\alpha_2 = 0.4$, whereas right panel shows the plots for extensile case with $\alpha_2 = -0.4$.

3.4 Discussions

We write the hydrodynamic equations of motion for active nematics suspended in an incompressible fluid called "active nematic gel". We study the effect of quenched disorder on the system kinetics and call it the random field wet active nematics or RFWAN. Results from the numerical simulation suggest that in RFWAN, finite disorder slows the defect annihilation kinetics that results in slow coarsening in the system. The effect of disorder is almost the same for both the contractile and extensile cases. The growth of the density field is faster compare to the nematic order parameter field. This is different from what we observed for dry-RFAN [Kumar & Mishra (2020)]. Further, the calculation of correlation length for a different amount of disorder suggests that the change in density growth is small compare to the growth of the nematic order parameter System shows good dynamics scaling for fixed disorder strength and both the contractile and extensile cases. Still, it does not show static scaling for different disorder strengths at a fixed time.